Dalton Transactions

ROYAL SOCIETY OF CHEMISTRY

COMMUNICATION

View Article Online
View Journal | View Issue

Cite this: *Dalton Trans.*, 2021, **50**, 17478

Received 13th June 2021,
Accepted 4th November 2021

DOI: 10.1039/d1dt01937f

rsc.li/dalton

Solvent-controlled elongation and mechanochemical strain in a metal–organic framework†

Aleksandra Półrolniczak, ‡[a] Szymon Sobczak, ‡[a] Varvara I. Nikolayenko,[b] Leonard J. Barbour *[b] and Andrzej Katrusiak *[a]

Under high pressure, crystals of $[Zn(m\text{-}btcp)_2(bpdc)_2]\cdot 2DMF\cdot H_2O$, referred to as DMOF are particularly sensitive to the type of pressure-transmitting media (PTM) employed: large PTM molecules seal the pores and DMOF is compressed as a closed system, whereas small PTM molecules are pushed into the pores, thereby altering the stoichiometry of DMOF. Compression in glycerol and Daphne 7474 leads to negative linear compressibility (NLC), while a mixture of methanol : ethanol : water 'hyperfills' the pores of the chiral framework, adjusting its 3-dimensional strain and resulting in pressure-induced amorphization around 1.2 GPa. The uptake of the small-molecule PTM strongly increases the dimensions of DMOF in the direction perpendicular to that of the NLC of the crystal.

Properties of porous metal–organic frameworks (MOFs) can be tailored specifically for applications such as gas storage and separation,[1] nanosensing,[2] catalysis of chemical reactions,[3] medical drug delivery[4] and others.[5] By combining flexible organic ligands with rigid inorganic nodes, we can construct structurally flexible MOFs with high thermal stability. However, under external stimuli, MOFs can undergo strong conformational changes resulting in phase transitions or even chemical reactions.[6–14] A thorough understanding of the mechanisms behind these structural rearrangements is essential for the rational design of new materials.

In response to various kinds of stimuli (*e.g.* light, heat, pressure and magnetic field), optoelectrical, optomechanical and optochemical effects are coveted for practical applications. Upon irradiation with light of a particular wavelength, the crystals of certain photochromic molecules change colour,[15,16] which is often accompanied by structural, electronic and even chemical rearrangements.[2,16] One of the most thoroughly investigated classes of compound comprises derivatives of bis-3-thienylcyclopentenes (*btcps*) capable of topochemical photocyclisation to form stable closed-ring isomers.[17,18] *Btcp* compounds were first employed for the construction of MOFs by Luo *et al.*[19] and later also by other groups.[20–24]

We previously reported a series of four MOFs prepared from $Zn(NO_3)_2$ and 1,2-bis[2-methyl-5-(4-pyridyl)-3-thienyl]-perfluorocyclopentene (*m-btcp*) or 1,2-bis[2-ethyl-5-(4-pyridyl)-3-thienyl]-perfluorocyclopentene (*e-btcp*), combined with either the rigid 4,4′-biphenyldicarboxylic acid (H_2bpdc) or the flexible 4,4′-oxybisbenzoic acid (H_2oba). Owing to ligand flexibility[25] and the degree of interpenetration, solid-state photocyclization only occurred in $[Zn(e\text{-}btcp)_2(oba)_2]$ (DMOF3) upon irradiation with 365 nm UV light.[23]

Extreme hydrostatic pressure is also a strong and efficient stimulus capable of inducing phase transitions,[26–28] enforcing the transport of molecules in porous materials[29–31] and even triggering chemical reactions.[26,32,33] Owing to their framework structures, MOFs can exhibit unique mechanochemical properties under such conditions (*e.g.*, negative linear expansion and negative area compressibility).[7,11,12,34] The applications that arise from this effects are of growing interest due to the development of pressure sensors and actuators for high-pressure underwater and geological installations, hydrothermal chambers, autoclaves and pressure reactors.[12,34] The generation of anisotropic compression in a material under hydrostatic stress is often related to the flexibility of linkers, which dominates the strain of the MOF's framework.[12] It should be stressed that the physical definition of compressibility is reserved for 'closed systems' of fixed stoichiometry and in one phase of the compound (compressibility should not be calculated across phase transitions). These conditions are fulfilled for the compression in large-molecule PTMs. However,

[a]*Department of Materials Chemistry, Faculty of Chemistry, Adam Mickiewicz University, Umultowska 89b, 61-614 Poznań, Poland. E-mail: katran@amu.edu.pl*
[b]*Department of Chemistry and Polymer Science, University of Stellenbosch, 7602, Matieland, South Africa. E-mail: ljb@sun.ac.za*

†Electronic supplementary information (ESI) available: Details regarding loading of the diamond anvil cell. CCDC 1956801–1956804, 1956866–1956870 for DMOF compressed in glycerol, 1956872–1956875 Daphne 7474 and 1956823–1956826, 1956193 for MEW. For ESI and crystallographic data in CIF or other electronic format see DOI: 10.1039/d1dt01937f

‡These authors contributed equally.

small-molecule PTMs can trigger the transport of guests to and from the pores and the stoichiometry of the sample crystal changes as a function of pressure. Such a sample, when exposed to high pressure, can even increase in volume due to the uptake of new guests.

In this context we now present structural data relating to the effects of hydrostatic pressure, involving different hydrostatic media, on single crystals of the 3D host framework $[Zn(m\text{-}btcp)_2(bpdc)_2]\cdot 2DMF\cdot H_2O$ (denoted as DMOF). DMOF crystallises in the orthorhombic space group $P2_12_12_1$. The central zinc ion is tetrahedrally coordinated to two *bpdc* dianions and two *m-btcp* molecules (Scheme 1). These units are interconnected to form a honeycomb-like topology composed of chiral four-connected nets with fivefold interpenetration.[23] The structure contains large guest-accessible channels extending along *a* (Fig. 1), with elliptical cross-sections that are elongated along *b*. The pores are easily accessible by small-solvent molecules, with the as-synthesised structure containing DMF and water guest molecules.

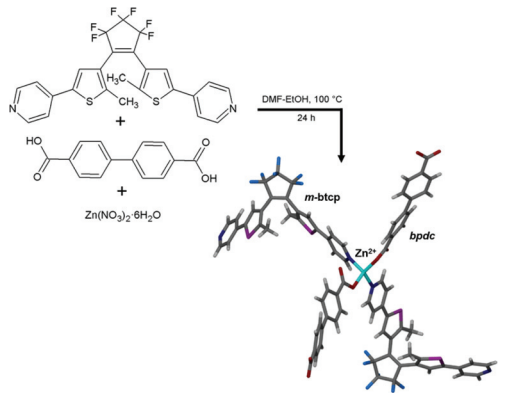

Scheme 1 Solvothermal preparation of DMOF from $Zn(NO_3)_2$, *m-btcp* and H_2*bpdc*.

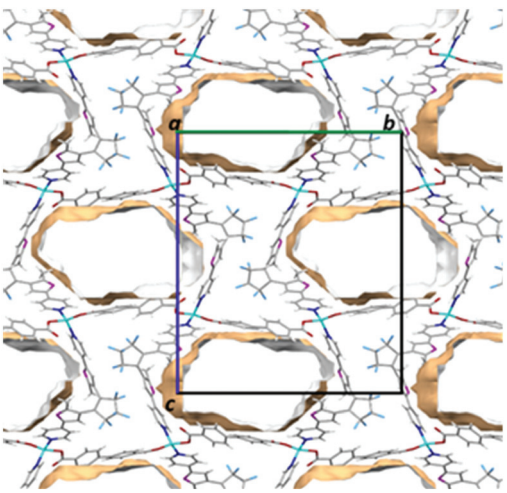

Fig. 1 Guest-accessible space (*ca.* 33% of the total volume) in the structure of DMOF as viewed along *a*; calculated using the program mercury[35] (probe radius 1.5 Å).

Since we had been unable to cyclise the *m-btcp* component of DMOF by means of photoirradiation, we elected to also investigate the effects of extreme compression for this purpose (see ESI† for details). Crystals of as-synthesised DMOF were loaded into a Merrill–Bassett diamond-anvil cell (DAC) and, owing to the presence of large channels, separate diffraction experiments were carried out using the non-penetrating hydrostatic fluids glycerol and Daphne 7474, or a penetrating mixture of methanol : ethanol : water (MEW). As a result, a straightforward mechanism linking the crystal structure and its compression (in the non-penetration PTMs) and mechanochemical strain (in penetrating PTM) can be elucidated. Relevant crystallographic parameters are summarised in Table 1. A common feature of hydrostatic compression of porous crystals is that the magnitude along the pores (here along *a*) is the least compressed/strained.[36]

In non-penetrating media DMOF is most compressed along *c* with $\beta_c = -1/c\cdot\partial c/\partial p = 24(5)$ TPa^{-1}, while negative linear compression (NLC) occurs along *b* (Fig. 2, 3 and Table S1†). The compressibility of −16(3) TPa^{-1} along *b*, calculated between 0.1 MPa and 1.7 GPa, corresponds to the elongation of this unit-cell dimension by 0.75 Å. The strong changes in *b* and *c* originate from the elliptical cross-section of the pores (the unit-cell parameters *b* and *c* are correlated to the semi-major and semi-minor axes of the pores, respectively). Although increasing pressure causes narrowing of the pore along its short cross-sectional dimension (*i.e.*, along *c*), the pores do not collapse. It is also important to note that the compressibilities along both *b* and *c* are linked owing to framework deformation (*i.e.*, the wine-rack mechanism hinged on the cations, and conformational changes in the ligands rather than on the metal cations only, which is typical of MOFs with rigid linkers[37,38]). In principle, the effect of the elliptical pores should be similar to that for discrete molecules (such as ROY, methanol monohydrate, POM, and others) and metal-hinged MOFs.

In the penetrating medium MEW, the mechanochemical strains along *b* and *c* are reversed compared to the compressibilities along these directions in non-penetrating PTMs (Fig. 2). The mechanochemical strain along *b* becomes positive ($\beta_b = 27(6)$ TPa^{-1}), while that along *c* is negative ($\beta_c = -44(3)$ TPa^{-1}), as calculated between structures at 0.1 MPa and 1.18 GPa (Fig. 2, 3 and Table S2†). This change is ascribed to the intake of new guest molecules, which 'inflate' the channels, thus causing elongation of *c* (*i.e.* along the semi-minor axis of the elliptical channel). Owing to wine-rack coupling through the framework, this shortens the semi-major axis of the channel along *b*.

The process of superfilling (or hyperfilling)[33] increases the initial unit-cell volume by about 100 Å^3 at 0.25 GPa (Fig. 2 and Table 1). This implies an intake (in volume) of approximately 5 non-hydrogen atoms per unit cell into the crystal structure, which corresponds to the *ca.* 74 additional electrons located within the pores, as estimated by the SQUEEZE subroutine of Platon. Further compression in MEW magnifies the adsorption

Table 1 Selected crystallographic data for DMOF and its clathrate with methanol : ethanol : water (M : E : W)

Pressure [GPa]	0.0001	0.19	0.8	1.5	0.25	0.56	0.85	1.18
Environment	Atmospheric	Daphne 7474	Glycerol	Glycerol	M : E : W	M : E : W	Me : E : W	M : E : W
Space group	$P2_12_12_1$	$P2_12_12_1$	$P2_12_12_1$	$P2_12_12_1$	$P2_12_12_1$	$P2_12_12_1$	$P2_12_12_1$	$P2_12_12_1$
a (Å)	7.11393(12)	7.011(17)	6.730(2)	6.513(9)	7.1001(8)	7.1015(18)	7.072(4)	7.029(3)
b (Å)	24.9253(4)	25.05(2)	25.256(15)	25.67(3)	24.68(2)	24.22(3)	24.225(15)	24.125(10)
c (Å)	29.0241(8)	28.81(5)	28.79(4)	27.96(7)	29.899(7)	30.248(17)	30.38(5)	30.55(4)
V (Å^3)	5146.45(19)	5059(16)	4893(7)	4675(14)	5240(5)	5202(8)	5205(10)	5181(8)
D_x [a] (g cm^{-3})	1.162	1.182	1.222	1.279	1.141	1.149	1.149	1.154
Z/Z'	4/1	4/1	4/1	4/1	4/1	4/1	4/1	4/1

[a] D_x – the initial stoichiometry $C_{39}H_{24}F_6N_2O_4S_2Zn{\cdot}C_3H_6NO$ was assumed and no water content was considered for the density calculations.

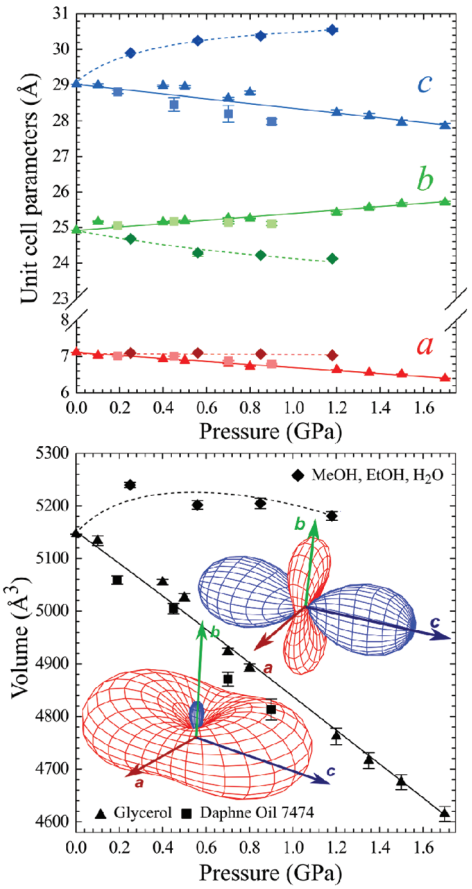

Fig. 2 Pressure dependence of the unit-cell parameters (top) and volume (bottom) for isothermal compression of DMOF in the non-penetrating oils Daphne 7474 (squares) and glycerol (triangles), and the penetrating MEW mixture (diamonds). The lines are for guiding the eye.

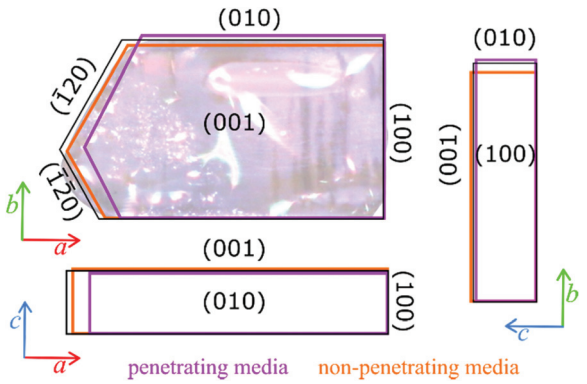

Fig. 3 Crystal contours (black) overlayed with a photo of a DMOF crystal (at 0.1 MPa), and the contours of this sample compressed in non-penetrating (orange, 1.20 GPa) and penetrating (purple, 1.18 GPa) media. The crystal contours are shown in three projections, to better represent the effect of negative linear compression (NLC) along the [*y*] direction (in non-penetrating media) and the activated expansion along the [*z*] direction (in penetrating media), respectively.

phenomenon, thus allowing additional molecules to penetrate the structure. This intake proceeds continuously until a pressure of 1.2 GPa is reached, after which the DMOF framework likely collapses; no diffraction pattern was observed above 1.2 GPa, suggesting that the crystal becomes amorphous. Analogous mechanochemical behaviour was also observed in other MOFs.[33] It is characteristic that the compression of DMOF crystals in non-penetrating PTM does not result in the amorphization or deterioration of the crystal quality, whereas the penetrating PTM leads to the crystal amorphization. This behaviour is different than that in most porous crystals, where the internal pressure of the PTM compressed inside the pores supports their walls, which precludes their collapse. It appears that the uptake of the PTM continues with pressure and at some point destabilize the framework, or that pressure higher than 1.2 GPa triggers shifts of the guests and collapses of portions of the pores.

Although we did not observe the hoped-for cyclisation of *m-btcp*, we have established that DMOF exhibits interesting mechanochemical behaviour when compressed in non-penetrating and penetrating media. Owing to the strong and inverse elastic responses between negative and positive deformation in two orthogonal directions, DMOF can be considered as a molecular sensor capable of detecting molecules of different sizes in its compressed environment. The most interesting property of DMOF is that its NLC in the non-penetrating media contrasts with the elongation along another direction in a penetrating PTM. This unique feature could be applied as a switch of sensors of fluids (operating under pressure, like in oil pipes) or micro mechanisms controlled by hydraulic systems. Certainly, a library of materials with such exceptional mechanical and mechanochemical properties is needed.

Conflicts of interest

There are no conflicts to declare.

Acknowledgements

AP, SS and AK are grateful to the Polish National Science Centre (grant OPUS 10 No. UMO-2015/19/B/ST5/00262). SS also thanks grant POWR.03.02.00-00-I023/17 and AP grant POWR.03.02.00-00-I026/16 co-financed by the European Union through the European Social Fund under the Operational Program Knowledge Education Development for the finical support. VIN and LJB thank the National Research Foundation (NRF) of South Africa for financial support.

Notes and references

1 H. Li, K. Wang, Y. Sun, C. T. Lollar, J. Li and H. C. Zhou, *Mater. Today*, 2018, **21**, 108–121.
2 E. A. Dolgopolova, A. M. Rice, C. R. Martin and N. B. Shustova, *Chem. Soc. Rev.*, 2018, **47**, 4710–4728.
3 J. Lee, O. K. Farha, J. Roberts, K. A. Scheidt, S. T. Nguyen and J. T. Hupp, *Chem. Soc. Rev.*, 2009, **38**, 1450–1459.
4 G. Férey, C. Serre, C. Kreuz, L. Cynober, Y. K. Hwang, T. Baati, P. Horcajada, T. Chalati, B. Gillet, S. Gil, P. Clayette, J.-S. Chang, D. Heurtaux, J. F. Eubank, P. Couvreur, C. Sebrie, R. Gref, P.-N. Bories and V. Marsaud, *Nat. Mater.*, 2009, **9**, 172–178.
5 H. C. J. Zhou and S. Kitagawa, *Chem. Soc. Rev.*, 2014, **43**, 5415–5418.
6 A. J. Graham, J. C. Tan, D. R. Allan and S. A. Moggach, *Chem. Commun.*, 2012, **48**, 1535–1537.
7 F. X. Coudert, *Chem. Mater.*, 2015, **27**, 1905–1916.
8 Z. Su, Y. R. Miao, G. Zhang, J. T. Miller and K. S. Suslick, *Chem. Sci.*, 2017, **8**, 8004–8011.
9 W. Cai and A. Katrusiak, *Nat. Commun.*, 2014, **5**, 4337.
10 A. Półrolniczak, S. Sobczak and A. Katrusiak, *Inorg. Chem.*, 2018, **57**, 8942–8950.
11 G. Tabacchi, *ChemPhysChem*, 2018, **19**, 1249–1297.
12 I. E. Collings and A. L. Goodwin, *J. Appl. Phys.*, 2019, **126**, 181101.
13 A. Lanza, L. S. Germann, M. Fisch, N. Casati and P. Macchi, *J. Am. Chem. Soc.*, 2015, **137**, 13072–13078.
14 P. Vervoorts, J. Keupp, A. Schneemann, C. L. Hobday, D. Daisenberger, R. A. Fischer, R. Schmid and G. Kieslich, *Angew. Chem.*, 2021, **133**, 800–806.
15 N. K. Kulachenkov, D. Sun, Y. A. Mezenov, A. N. Yankin, S. Rzhevskiy, V. Dyachuk, A. Nominé, G. Medjahdi, E. A. Pidko and V. A. Milichko, *Angew. Chem., Int. Ed.*, 2020, **59**, 15522–15526.
16 R. Pardo, M. Zayat and D. Levy, *Chem. Soc. Rev.*, 2011, **40**, 672–687.
17 S. Kobatake, K. Uchida, E. Tsuchida and M. Irie, *Chem. Commun.*, 2002, **2**, 2804–2805.
18 D. Kitagawa, H. Nishi and S. Kobatake, *Angew. Chem., Int. Ed.*, 2013, **52**, 9320–9322.
19 F. Luo, C. B. Fan, M. B. Luo, X. L. Wu, Y. Zhu, S. Z. Pu and W. Xu, *Angew. Chem., Int. Ed.*, 2014, **53**, 9298–9301.
20 D. E. Williams, J. A. Rietman, J. M. Maier, R. Tan, A. B. Greytak, M. D. Smith, J. A. Krause and N. B. Shustova, *J. Am. Chem. Soc.*, 2014, **136**, 11886–11889.
21 H. Sato, R. Matsuda, S. Kitagawa, Y. Zheng, H. J. Jeon and P. Wu, *Nat. Commun.*, 2017, **8**, 100.
22 K. Matsuda, K. Takayama and M. Irie, *Inorg. Chem.*, 2004, **43**, 482–489.
23 V. I. Nikolayenko, S. A. Herbert and L. J. Barbour, *Chem. Commun.*, 2017, **53**, 11142–11145.
24 Y. Zheng, H. Sato, P. Wu, H. J. Jeon, R. Matsuda and S. Kitagawa, *Nat. Commun.*, 2017, **8**, 100.
25 S. Sobczak, A. Półrolniczak, P. Ratajczyk, W. Cai, A. Gładysiak, V. I. Nikolayenko, D. C. Castell, L. J. Barbour and A. Katrusiak, *Chem. Commun.*, 2020, **56**, 4324–4327.
26 A. Katrusiak, *Acta Crystallogr., Sect. B: Struct. Sci., Cryst. Eng. Mater.*, 2019, **75**, 918–926.
27 P. G. Yot, Q. Ma, J. Haines, Q. Yang, A. Ghoufi, T. Devic, C. Serre, V. Dmitriev, G. Férey, C. Zhong and G. Maurin, *Chem. Sci.*, 2012, **3**, 1100–1104.
28 C. L. Hobday, C. H. Woodall, M. J. Lennox, M. Frost, K. Kamenev, T. Düren, C. A. Morrison and S. A. Moggach, *Nat. Commun.*, 2018, **9**, 1–9.
29 A. J. Graham, D. R. Allan, A. Muszkiewicz, C. A. Morrison and S. A. Moggach, *Angew. Chem., Int. Ed.*, 2011, **50**, 11138–11141.
30 S. A. Moggach, T. D. Bennett and A. K. Cheetham, *Angew. Chem.*, 2009, **121**, 7221–7223.
31 K. W. Chapman, G. J. Halder and P. J. Chupas, *J. Am. Chem. Soc.*, 2009, **131**, 17546–17547.
32 S. Sobczak and A. Katrusiak, *Inorg. Chem.*, 2019, **58**, 11773–11781.
33 S. C. McKellar and S. A. Moggach, *Acta Crystallogr., Sect. B: Struct. Sci., Cryst. Eng. Mater.*, 2015, **71**, 587–607.
34 A. B. Cairns and A. L. Goodwin, *Phys. Chem. Chem. Phys.*, 2015, **17**, 20449–20465.
35 C. F. Macrae, I. J. Bruno, J. A. Chisholm, P. R. Edgington, P. Mccabe, E. Pidcock, L. Rodriguez-monge, R. Taylor, J. Van De Streek and P. A. Wood, *J. Appl. Crystallogr.*, 2008, **41**, 466–470.
36 J. C. Tan, T. D. Bennett and A. K. Cheetham, *Proc. Natl. Acad. Sci. U. S. A.*, 2010, **107**, 9938–9943.
37 A. U. Ortiz, A. Boutin, A. H. Fuchs and F.-X. Coudert, *J. Chem. Phys.*, 2013, **138**, 174703.
38 S. M. J. Rogge, M. Waroquier and V. Van Speybroeck, *Acc. Chem. Res.*, 2018, **51**, 138–148.